

# Ocean surface waves in an ice free Arctic Ocean

**Jian-Guo Li**

*Met Office, Exeter EX1 3PB, United Kingdom*

*Email: Jian-Guo.Li@metoffice.gov.uk*

**Abstract:** The retreating of Arctic ice edge implies that global ocean surface wave models have to be extended at high latitudes or even to cover the North Pole in the future. The obstacles for conventional latitude-longitude grid wave models to cover the whole Arctic are the polar problems associated with their Eulerian advection schemes, including the CFL restriction on diminishing grid-length towards the Pole, the singularity at the Pole and the invalid scalar assumption for vector components defined relative to the local east direction. A spherical multiple-cell (SMC) grid is designed to solve these problems. It relaxes the CFL restriction by merging the longitudinal cells towards the Poles. A round polar cell is used to remove the singularity of the differential equation at the Pole. A fixed reference direction is used to define vector components within a limited Arctic part in order to reduce the scalar assumption errors at high latitudes. The SMC grid has been implemented in the WAVEWATCH III model and validated with altimeter and buoy observations, except for the Arctic part, which could not be fully tested due to a lack of observations as the polar region is still covered by sea ice. Here an idealised ice free Arctic case is used to test the Arctic part and it is compared with a reference case with real ice coverage. An expanded Arctic part is also used for comparisons of the Arctic part with available satellite measurements. It also provides a direct model comparison of the two reference systems in their overlapping zone.

## 1. Introduction

The Arctic sea ice coverage has shrunk at alarming speeds in recent summers and climate scientists have predicted an essentially ice-free Arctic summer in the near future (Wang and Overland, 2009). For instance the Arctic ice edge retreated to as high as 86° N in summers of 2007 and 2012. This change, and a foreseen requirement to forecast sea-state in support of marine operations in the Arctic, has prompted ocean surface wave models to extend at high latitudes or even to include the North Pole. The major problem in extending a latitude-longitude (lat-lon) grid wave model at high latitudes is the diminishing longitude grid-length towards the Pole, which exerts a severe restriction on time steps of finite-difference schemes. Another problem is the increased curvature of the parallels at high latitudes, which erodes the scalar assumption of vector components defined relative to the local east direction, such as the meridian and zonal velocity components. Wave energy spectra in ocean surface wave models are discretised into directional components relative to the local east so they face the same scalar assumption problem as the velocity components at high latitudes.

Among various grids developed to tackle the polar problems, the spherical multiple-cell (SMC) grid (Li, 2011) is an efficient approach because it uses the same lat-lon grid cells and hence requires minimal changes to the lat-lon grid finite-difference schemes. The SMC grid relaxes the Courant-Friedrichs-Lewy (CFL) restriction of the Eulerian advection time-step by merging longitudinal cells

towards the Poles as in the reduced grid (Rasch, 1994). The merged cells also mitigate the restriction on diffusion time steps (Fourier number less than one) as a diffusion term usually accompanies an advection scheme to smooth the so called garden sprinkler effect of a discrete wave spectrum (Booij and Holthuijsen, 1987). Round polar cells are introduced to remove the polar singularity of the spherical coordinate system. Vector component propagation errors caused by the scalar assumption at high latitudes are reduced by replacing the local east with a fixed reference direction to define the wave spectral components in the Arctic.

The SMC grid has been implemented into the WAVEWATCH III model (WW3, Tolman, 1991; Tolman et al., 2002; Tolman and WDG, 2014) and has been validated with classic numerical tests (Li, 2011) and ocean surface wave observations (Li, 2012). However, the Arctic part, in which a fixed reference direction is used to maintain the scalar assumption, cannot be fully tested against observations in the polar region as it is still covered by sea ice. This paper will use an idealised ice-free case to illustrate the SMC grid performance in the Arctic polar region. An expanded Arctic part is also used so that it covers some open sea surface and can then be compared with satellite observations. By comparing the expanded Arctic part model with the original Arctic part, the two reference direction systems can then be compared directly within their overlapping area. Buoy wave spectral observations are also used for this validation study to ensure the consistency of the global model.

## 2. SMC grid Arctic part

Numerical schemes for propagation of ocean surface waves on the SMC grid are almost identical to those used on a conventional lat-lon grid because they share the same type of lat-lon mesh (Li, 2012). So in the polar region a SMC grid faces the same singularity and directionality problems as a lat-lon grid. To remove the singularity at the North Pole, a polar cell centred at the North Pole is introduced in the SMC grid so that the singular differential equation is replaced with an integral one for the polar cell. To mitigate the degrading of the scalar assumption of vector components due to the rapid changing local east direction at high latitudes, a fixed reference direction, the *map-east*, is used to define vector components above given latitude,  $\varphi_A$ , in the north polar region. This polar region using the map-east reference direction is called the *Arctic part* of the SMC grid. For convenience, the rest of the SMC grid which uses the conventional local east reference direction will be referred to as the *global part*.

The map-east reference direction can be approximated by a rotated grid with its rotated pole at 180°E on the Equator. The angle from this approximated map-east to the local east at longitude  $\lambda$  and latitude  $\varphi$  within the Arctic part is given by:

$$\alpha = \text{sgn}(\cos \varphi \sin \lambda) \arccos \left[ \frac{\cos \lambda \sin \varphi}{\sqrt{1 - (\cos \lambda \cos \varphi)^2}} \right]. \quad (1)$$

Please note the polar cell does not have a local east direction so the map-east angle (1) is undefined at the North Pole. To define the polar cell wave spectrum in the map-east system, the map-east angle is chosen to be zero, which is equivalent to use a value with  $\lambda = 0$  and  $\varphi$  slightly less than  $\pi/2$  in (1). This missing local east at the North Pole does not affect the SMC grid propagation scheme as it is formulated in a C-grid style, that is, only the meridian velocity component at the edge of the polar cell is required (Li, 2011).

Because the angle from the map-east to the local east varies with latitude and longitude, there are no fixed corresponding spectral components between the two systems. For this reason, wave spectra defined by local east cannot be mixed up with those defined from the map-east within the Arctic part. To separate these two parts in propagation schemes, the four rows just below the Arctic

part are duplicated and attached to the Arctic part. The Arctic part is then treated as an isolated region with a virtual coastline at the edge of the outmost boundary cells. Similarly, the global part is treated as if it has a coastline at its north edge. To link up these two parts, the lower two boundary rows in the Arctic part are updated with wave spectra from the corresponding cells in the global part after they are rotated anticlockwise by  $\alpha$ . For the global part, the top two rows are updated with wave spectra from the overlapping cells in the Arctic part after they are rotated clockwise by  $\alpha$ . This overlapping boundary treatment is similar to the two-way nesting (Tolman, 2008) except that different spectral reference directions are used in the two parts here.

Fig.1 shows the Arctic and European regions of a multi-resolution (3-6-12-25 km) SMC grid, which is defined with a base resolution of about 25 km lat-lon grid (a longitude increase of  $\Delta\lambda = 360^\circ/1024 = 0.3515625^\circ$  and a latitude increase of  $\Delta\phi = 180^\circ/768 = 0.234375^\circ$ ). The cells are merged longitudinally at high latitudes to relax the CFL restriction as described in (Li, 2011). Near coastlines cells are refined similar to the quadtree mesh refinement (Popinet et al 2010) by two more levels (12 and 6 km) except for in the European region, where it uses 3 refined levels (12-6-3 km). This grid has been prepared for global and regional ocean surface wave forecasting in the Met Office (Li and Saulter, 2014) and will be referred to as the SMC36125 grid. The Arctic part (marked by the red circle in Fig.1) is chosen above  $85^\circ\text{N}$  and the global part ends at about  $86^\circ\text{N}$  (as indicated by the golden circle in Fig.1) so that the Arctic part may not be used at all at present because it is still covered by sea ice almost all year around. Because of the unstructured nature of the SMC grid, the Arctic cells are appended after the global part in a single cell list for propagation. The two parts can then be conveniently separated by sub-loops and it is also convenient to switch off the Arctic part. The overlapping boundary rows are treated in the same way as other cells so the propagation is calculated together for both parts in a single loop. This allows maximum optimisation in parallel computations. Only the boundary cell update has to be treated as an extra calculation after each propagation time step.

Wind forcing for the Arctic part has to be converted into the map-east system as well. The conversion between the two systems uses the following transform:

$$\begin{pmatrix} u' \\ v' \end{pmatrix} = \begin{pmatrix} \cos \alpha & -\sin \alpha \\ \sin \alpha & \cos \alpha \end{pmatrix} \begin{pmatrix} u \\ v \end{pmatrix}, \quad \begin{pmatrix} u \\ v \end{pmatrix} = \begin{pmatrix} \cos \alpha & \sin \alpha \\ -\sin \alpha & \cos \alpha \end{pmatrix} \begin{pmatrix} u' \\ v' \end{pmatrix} \quad (2)$$

where  $u'$  and  $v'$  are the map-east velocity components,  $u$  and  $v$  are the corresponding local east velocity components, and the cosine and sine of the map-east angle are given by

$$\cos \alpha = \frac{\cos \lambda \sin \phi}{\sqrt{1 - (\cos \lambda \cos \phi)^2}}, \quad \sin \alpha = \frac{\sin \lambda}{\sqrt{1 - (\cos \lambda \cos \phi)^2}}, \quad (3)$$

Propagation of each wave component is calculated together for both global and Arctic parts with the same propagation scheme except that the zonal and meridian group velocity components for the Arctic part are given by

$$u = c_g \cos(\theta' - \alpha), \quad v = c_g \sin(\theta' - \alpha) \quad (4)$$

where  $\theta'$  is the spectral component angle from the map-east direction. Due to the fixed reference direction, the component propagation direction is also fixed as well in the Arctic part. The great circle turning (GCT) term (see Eq. 8 in Li, 2012) has to be modified in the Arctic part to use the rotated grid latitude, which is close to zero in the Arctic part because the rotated Equator passes the North Pole.

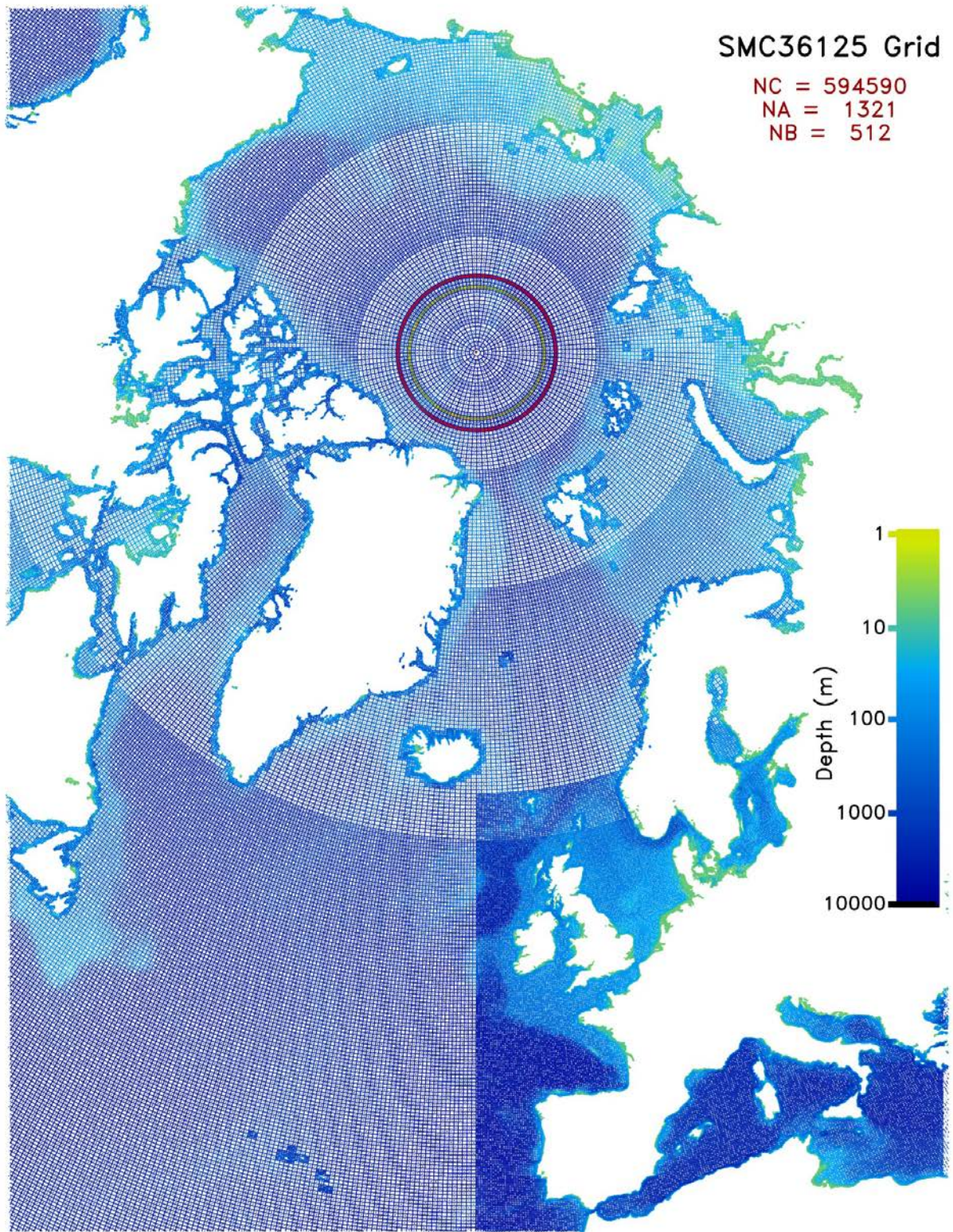


Fig.1. The Arctic and European regions of the SMC36125 grid.

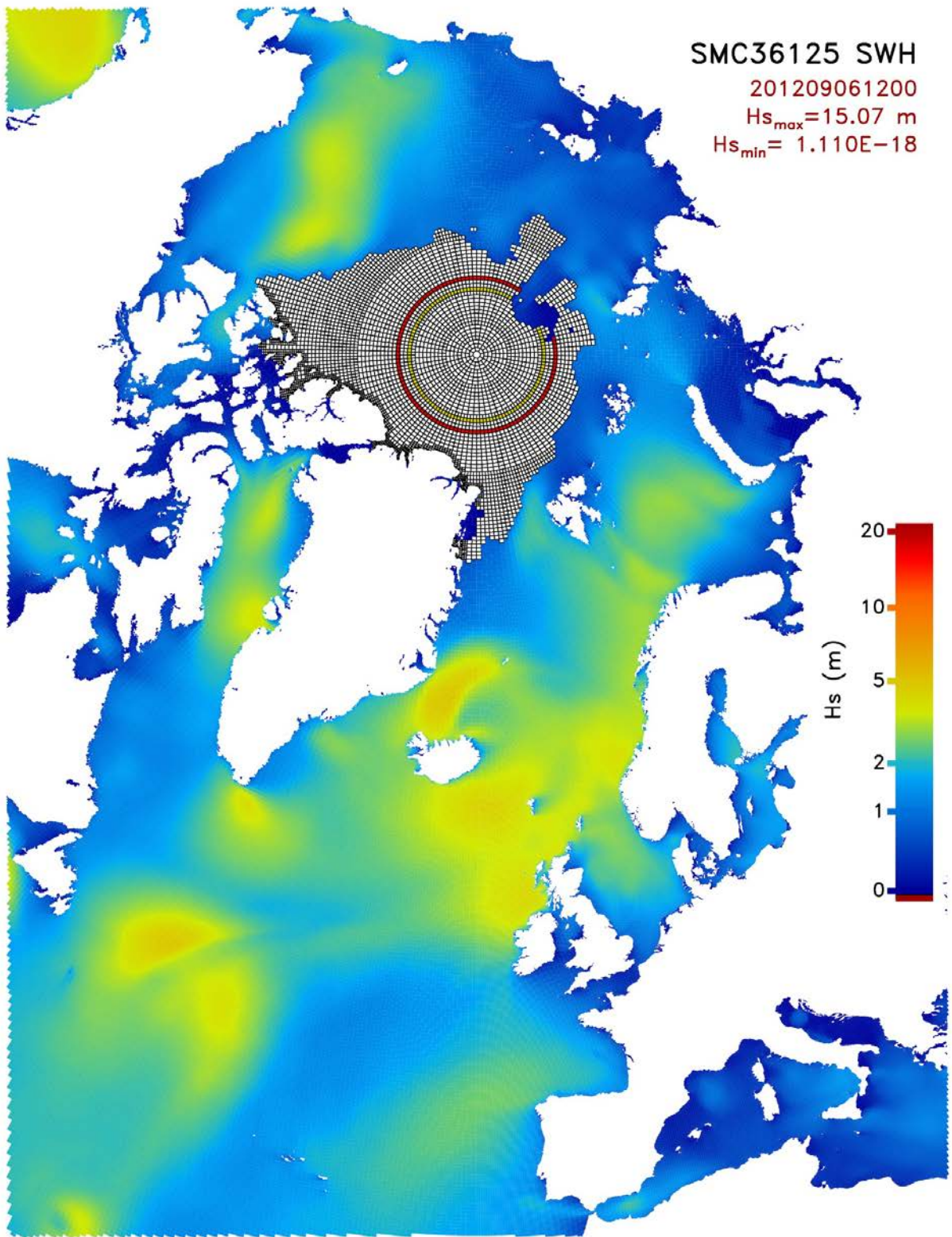


Fig.2. SWH from the SMC36125 grid wave model on 6 September 2012.

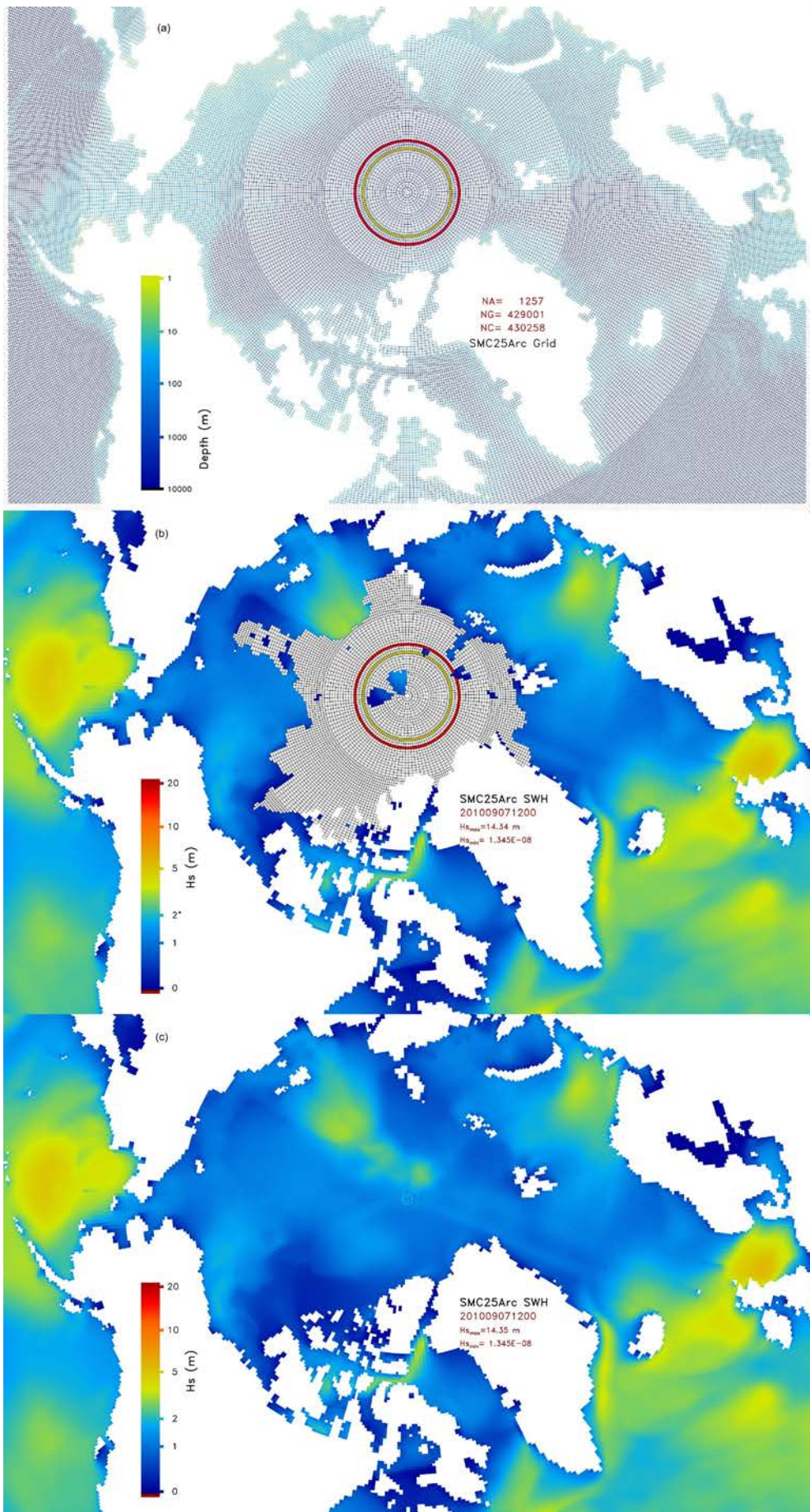


Fig.3. SMC25Arc grid (a) and SWH fields for ice (b) and ice-free (c) cases.

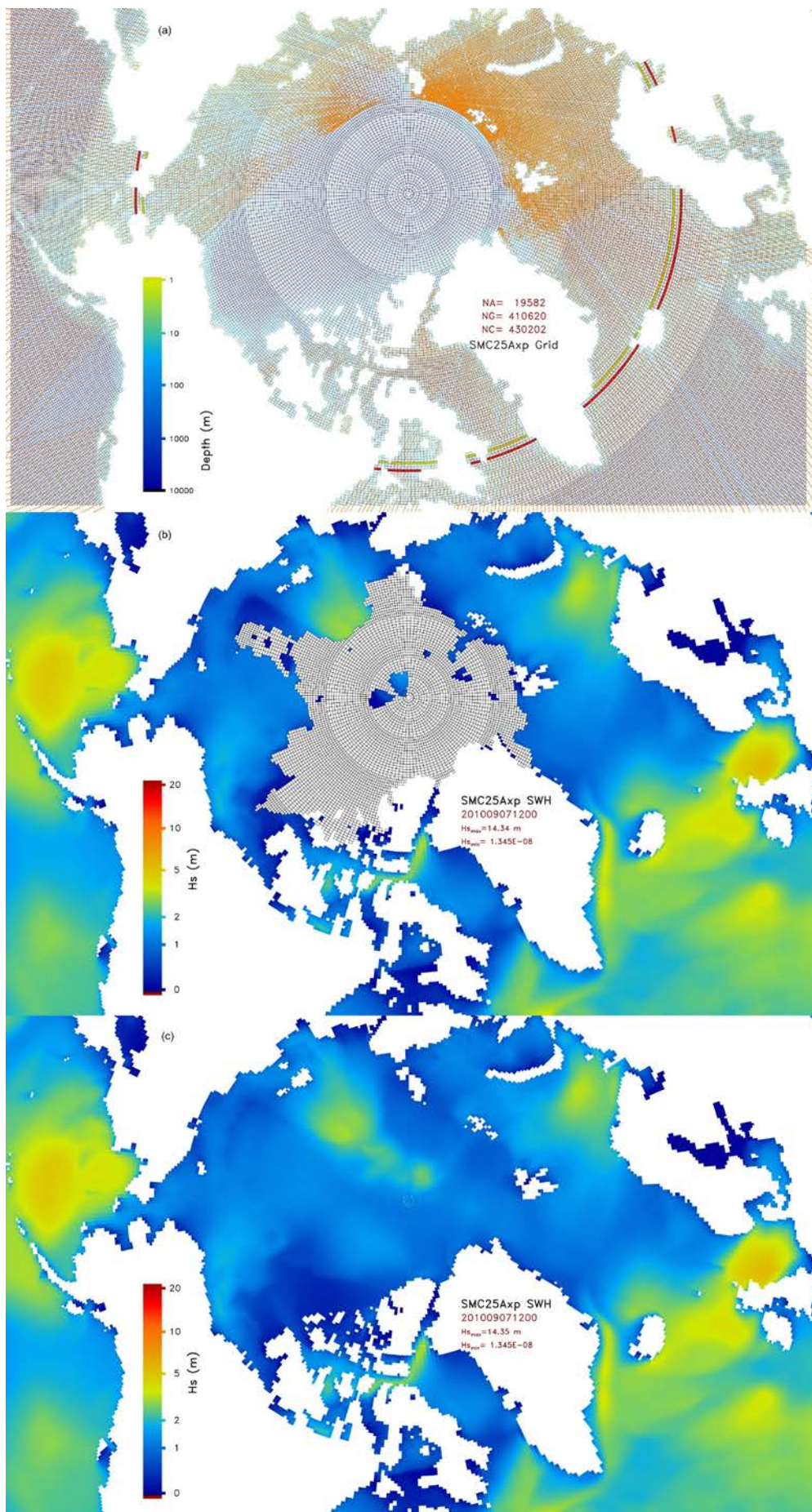


Fig.4. Same as Fig.3 but with expanded Arctic part. Satellite data points are overlaid in (a).

If the Arctic part is kept small around the polar region (like above 85°N in the SMC36125 grid), this GCT term becomes negligible. The refraction term (see Eq. 7 in Li, 2012) retains the formulation in the Arctic part except for that the gradients of water depth and current component along the wave direction have to be rotated to the map-east system. As the Arctic Ocean above 85°N is considered deep for wind waves, the refraction is also negligible in the small Arctic part.

A typical significant wave height (SWH) field from this model is shown in Fig.2 for 6 September 2012 when the Arctic sea ice coverage is close to the annual minimum. This figure is drawn cell by cell with a resolution of 250 colours within the SWH range from 0 to 22 m and it demonstrates the smooth transfer between different resolution cells, such as the refined coastlines, the European region and the merged cells at high latitudes. The Arctic part is activated in this case because a tongue of open sea surface has extended into the Arctic part. Nevertheless, most of the Arctic part is still covered by sea ice even at the minimum ice coverage time so it is difficult to validate the fixed reference direction method with any observations within this Arctic part.

### 3. Expanded Arctic part

For validation of the map-east reference direction method with some satellite observations available in the Arctic, the Arctic part is expanded from the original 85°N to about 65°N (see Fig.4a). As SMC grid cells have to be sorted by their sizes (in order to use sub-time steps for refined cells), base-resolution cells are listed at the end. The Arctic part cells are currently appended at the end of the full cell list (for the convenience of switching it off) so they have to be at the base-resolution. To ensure the expanded Arctic part (Axp) is still at the base-resolution, the refinement near coastlines is suspended and a single resolution (25km) SMC grid is used for the Axp model. Another SMC grid at the same single resolution but with the original Arctic part (Arc) is also used for comparison purpose (see Fig.3a). These single resolution grids will be referred to as SMC25 Arc and Axp, respectively.

The test period was chosen to be August-September 2010 for available Envisat satellite ocean surface wave measurements. Satellite data points in the two months are overlaid on the Axp grid (Fig.4a orange dots) and they cover a fair area of the Axp Arctic part. Two weeks were allowed for the models to spin up (from 1 August 2010) before comparing with satellite data. For comparison purposes, both models with the Arc and Axp configurations are run twice over the same period: one run with a normal ice fraction and another run ice-free. The ice-free runs are used to demonstrate how the map-east method handles the ocean surface wave propagation in the whole Arctic. The normal ice cases are used for comparisons with satellite data. Besides, the two reference direction systems can be compared directly in the overlapping area between the global part of the Arc grid and the Arctic part of the Axp grid (i.e. between 65°N and 85°N), where the two different systems are used in the two configurations, respectively.

The source terms for this study use a locally tuned version of the WW3 ST4 scheme (Ardhuin et al. 2010). An hourly 25 km spatial resolution surface ice fraction and wind forcing from the Met Office operational atmospheric model are used to drive the WW3 wave model. An upstream non-oscillatory 2nd order (UNO2) advection scheme (Li, 2008), adapted from the MINMOD scheme (Roe, 1985), is combined with a 2nd order diffusion term similar to (Booij and Holthuijsen, 1987) for wave transportation on the SMC grid. Partial sub-grid blocking similar to (Tolman, 2003) is used for the single resolution SMC25 grids. Wave refraction and GCT terms are estimated with a rotation scheme, which is free from the CFL restriction but subject to the physical limit of maximum refraction angle up to the local gradient direction (Li, 2012). The combined refraction and GCT term is switched off in the Arctic part in the WAVEWATCH III V4.18 public release code because it is negligible within the original small Arctic part. For this study with the expanded Arctic part, the GCT and refraction terms are turned on in the Arctic part to rule out any possible differences caused by these terms.

#### 4. Validation of Arctic part

Fig.3b and 4b show the modelled SWH from the SMC25 Arc and Axp models with real sea ice on 7 September 2010, when the Arctic sea ice coverage is at approximately the annual minimum. The ice edge was mostly below 83°N that year but some temporary polynas were present above 83°N and even inside the original Arctic part (Fig.3b). Fig.3c and 4c show the modelled SWH on the same date, but with the sea ice switched off. These ice-free runs allow the surface waves to travel freely over the whole Arctic Ocean, producing an ideal example for comparison of the two reference direction methods. The two runs generated almost identical SWH fields by visual comparison of Fig.3 and Fig.4 for both ice and ice-free cases. The transition between the global and Arctic parts is continuous and smooth for both models, implying that both the local-east and map-east systems works almost equally well in the overlapping area between 65°N and 85°N.

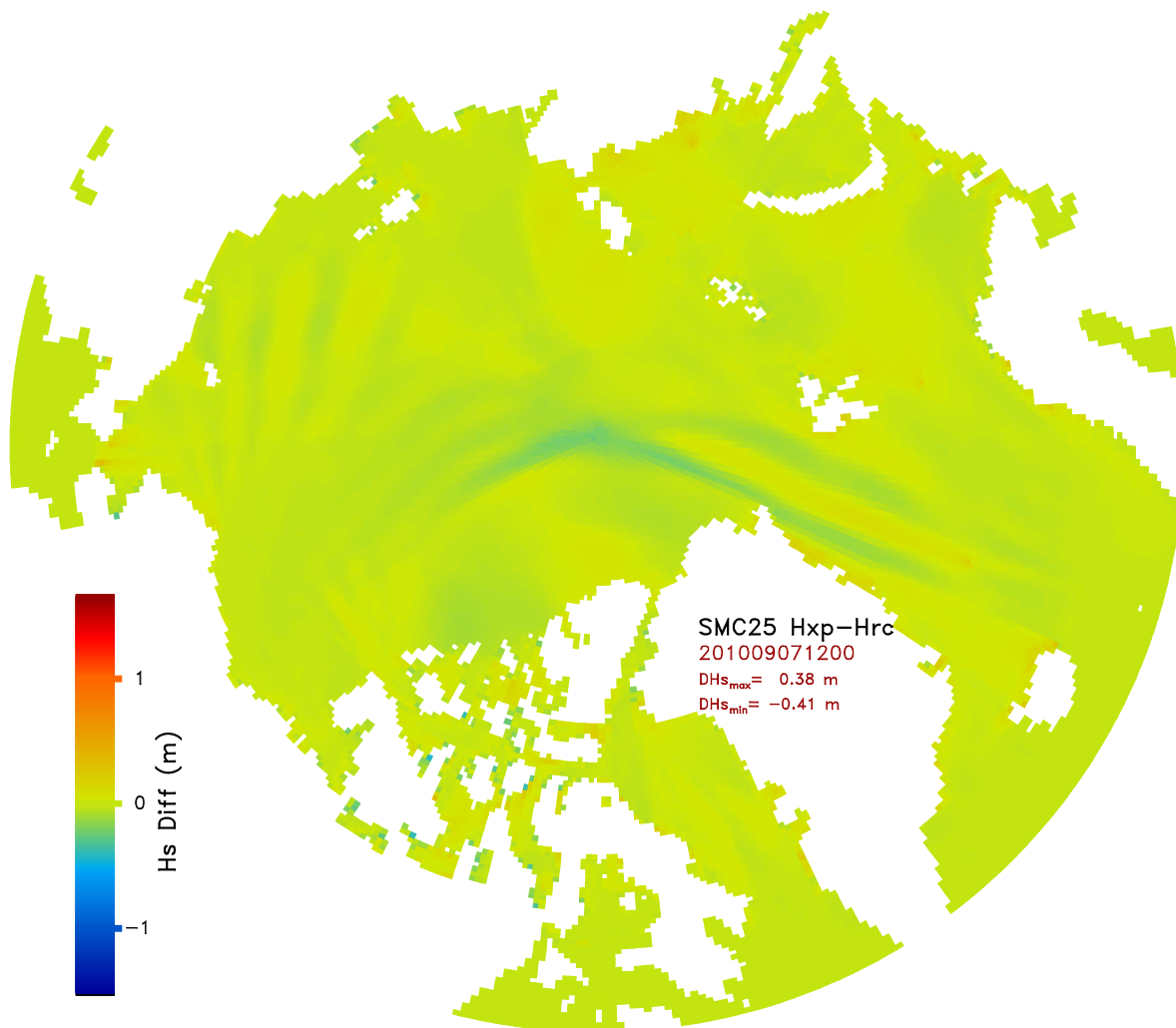


Fig.5. SWH difference between the Axp and Arc models on 20100907 1200 hr above 60°N.

Some subtle differences could be found between the two models in the expanded Arctic part as shown by the SWH difference between the two models in Fig.5 for the ice-free cases (Fig.3c and Fig.4c). Fig.5 covers the area above 60°N so that both Arctic transition zones (around 65°N for the Axp model and 85°N for the Arc model) are included. The SWH from the two models are almost identical below 66°N, confirming that the transition between the Axp Arctic and global parts is smooth. The difference within the Axp Arctic part shows striped patterns parallel with swell paths, indicating that the difference is caused by swells displaced by the two different systems. As the

curvature related errors in the local east system increases with latitude and becomes too large near the Pole, it is not a surprise that the two systems have some numerical differences in the overlapping region. Nevertheless, the differences are quite small and only become noticeable along swell paths. Note that the transition between the two parts of the Arc model is also continuous and smooth as there are no abrupt changes along the boundary circles around 85°N.

Differences between the ice and ice-free cases in the same Arc or Axp grid are primarily caused by the extended fetch lengths in the ice-free case. For instance, the waves from the Atlantic may reach the Bering Strait across the ice free Arctic Ocean. It could be envisaged that Arctic coastlines would expect more swell energy if the sea ice disappears in future summers. Most ice-free effects, however, will be restricted within the Arctic as the ice-covered region is almost sheltered by the Arctic coastlines from other oceans. It has to be stressed that attributing this small difference in such a complicated model to a definite cause is risky because a lot of processes are related and difficult to isolate. For example, advection, refraction and GCT schemes all have their inherent numerical diffusions, which depend on their speeds and directions (Li 2008). Any change in the transported field would result in changes in these numerical diffusions. These changes could not be easily pin-pointed or conveniently isolated from each other. Furthermore, source terms also depend on wave spectra and their effect may change as well if the wave changes.

For an objective assessment of the Arctic part performance, SWH observations from the radar altimeter (RA2) on board the European Space Agency (ESA) Envisat satellite are used for model validation. The satellite data are collocated with interpolated model values to minimise modification of the satellite data. This allows extra filters to be applied on the satellite data if required. For instance, spurious large satellite SWH values near coastlines pass through the ESA recommended filters but can be filtered out by comparing them to the interpolated model values (Li and Holt, 2009; Li and Saulter, 2012). Fig.6 compares the model and RA2 SWH along three satellite tracks, one crossing the Atlantic (*a*) and the other two passing the Pacific (*b* and *c*). They all span from the Southern Oceans to the Arctic. The blue '+' symbols indicate the RA2 measurements. Some spurious large satellite values are shown close to coastlines or ice edges. These large outliers are difficult to remove with available data parameters so a simple filter,  $SWH_{\text{satellite}} - SWH_{\text{model}} < 4$  m, is introduced to mitigate their effect on the statistics. There are three model values comparing with each RA2 entry: the SMC25 Arc (orange ×), Axp (red ×), and the SMC36125 (green +) model SWH values. The Arc and Axp model values are almost overlapped along all the three tracks, including the Arctic sections. This confirms that the two reference direction methods are consistent in the Arctic in both the original Arc and expanded Axp cases. The SMC36125 model shows a slightly better agreement with the Satellite data, particularly on the last Pacific track (*c*). This track (centred at 217°E 4°S) passes over the French Polynesia region in the Pacific, where the small coral reefs are not resolved by the 25 km grid. The SMC36125 grid has 6 km refined resolution in this region and can resolve some of the small islands, hence a better blocking effect on swell than the SMC25 model.

Fig.7 show the model-satellite scatter plots for the Arc (*a*) and Axp (*b*) models, respectively, over a 46-day period from 15 August to 30 September 2010. Only the satellite data in the expanded Arctic region (above 65°N) are used in Fig.7 in order to highlight the statistical differences between the two systems. Note that there are no satellite observations above about 83°N so the comparison is effectively limited within the overlapping zone. As a result, Fig.7 can be considered as an equivalent direct comparison of the two systems via the intermediate satellite data. Over 94,700 satellite entries are selected in this temporal and spatial slot and the model differences are really small. In fact, both models produce similar correlations (0.738 and 0.737) and rms errors (0.652 and 0.655 m) against the same satellite measurement. Although the Arc model shows slightly better than the Axp model in correlation and rms errors, the Axp model mean (1.432 m) is closer to the satellite one (1.499) than that of the Arc model (1.417). So it is hard to judge which method is better within the overlapping zone based on this comparison.

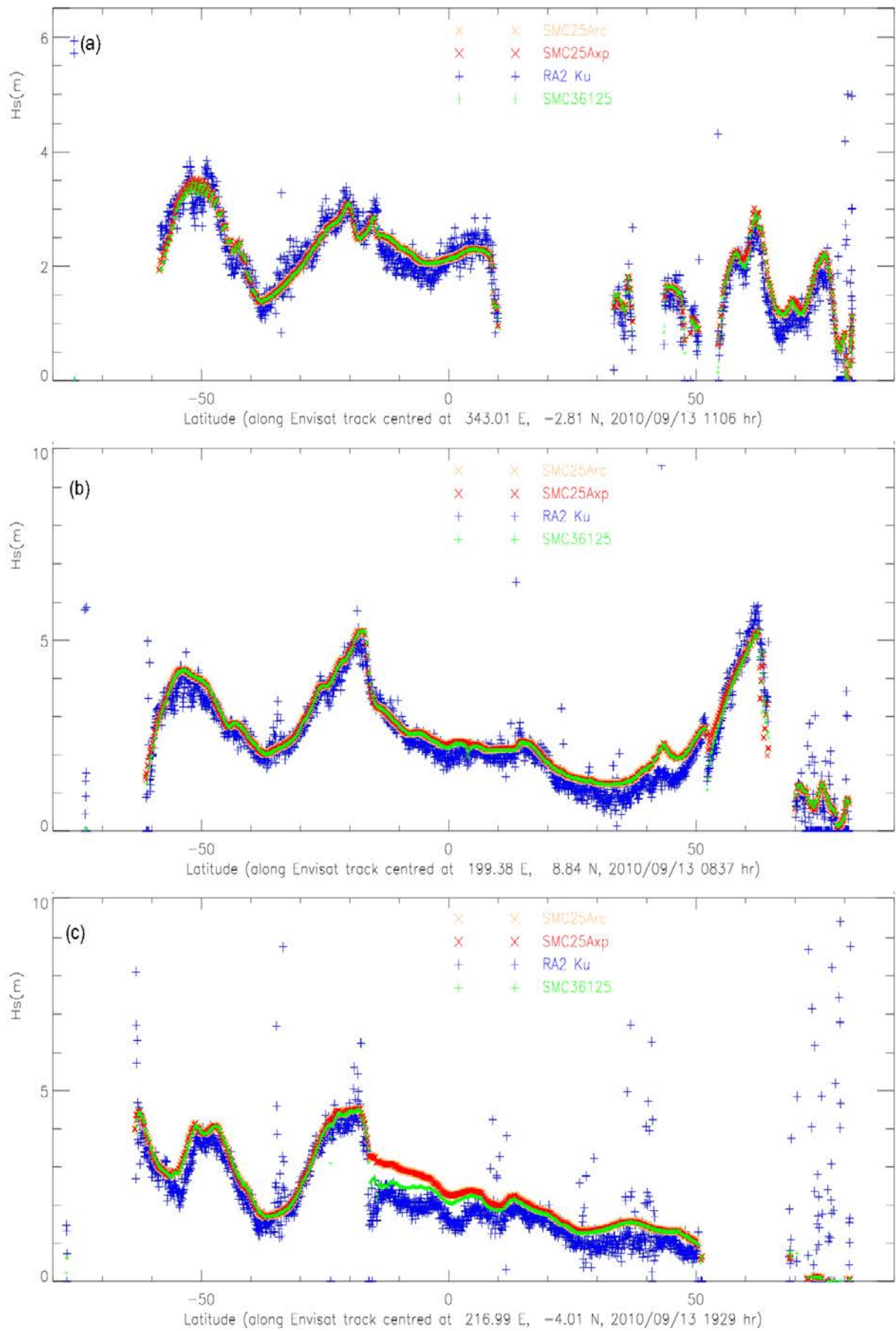


Fig.6. Comparison of SWH from 3 models with RA2 data along 3 Envisat satellite tracks.

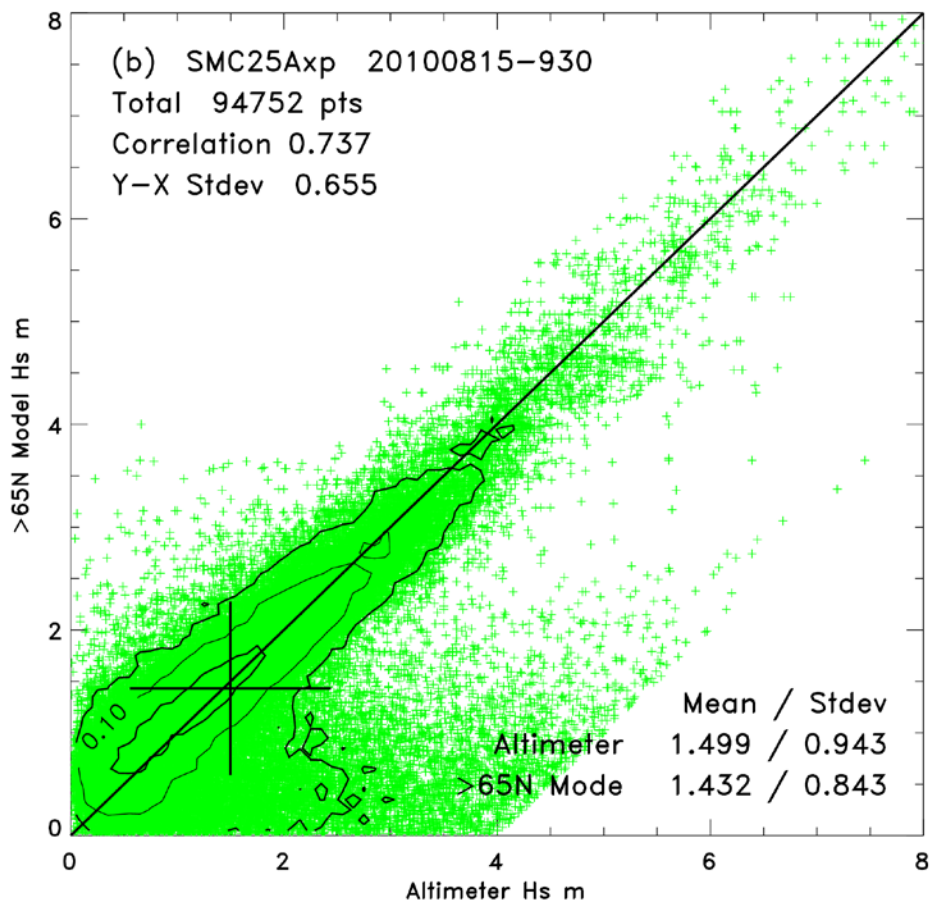
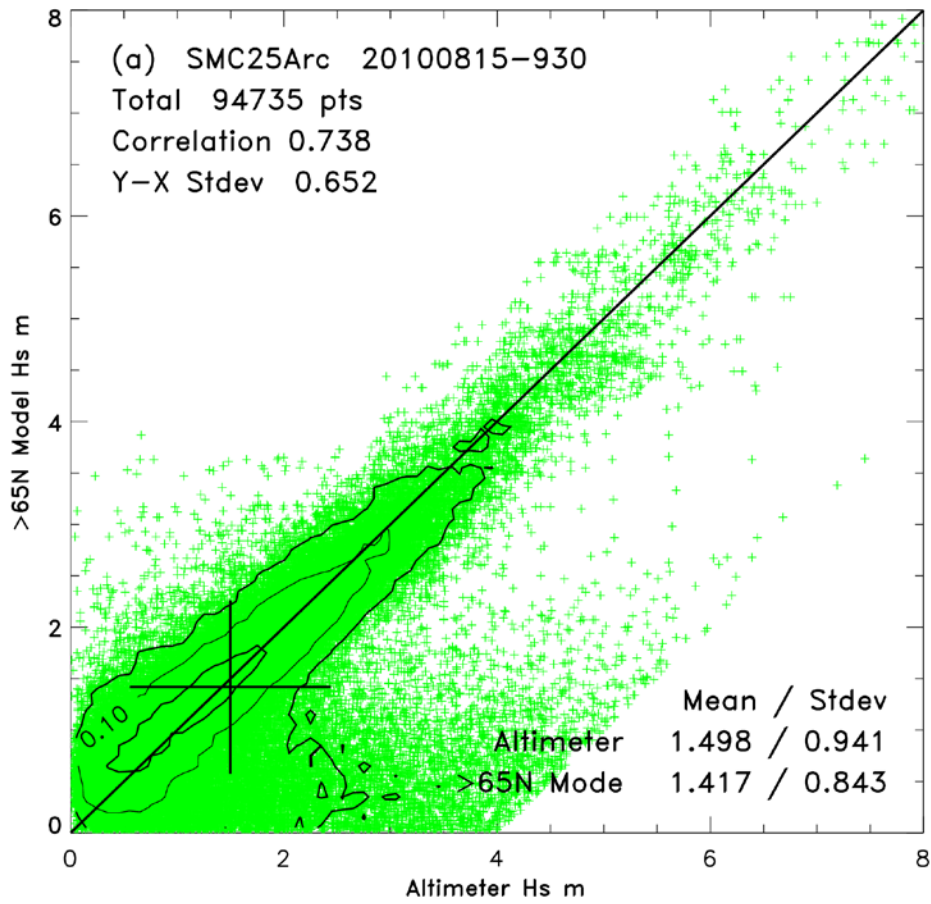


Fig.7. Comparison of SMC25Arc (a) and SMC25Axp (b) model SWH with Envisat altimeter data from 15 August to 30 September 2010 in the polar region above 65°N.

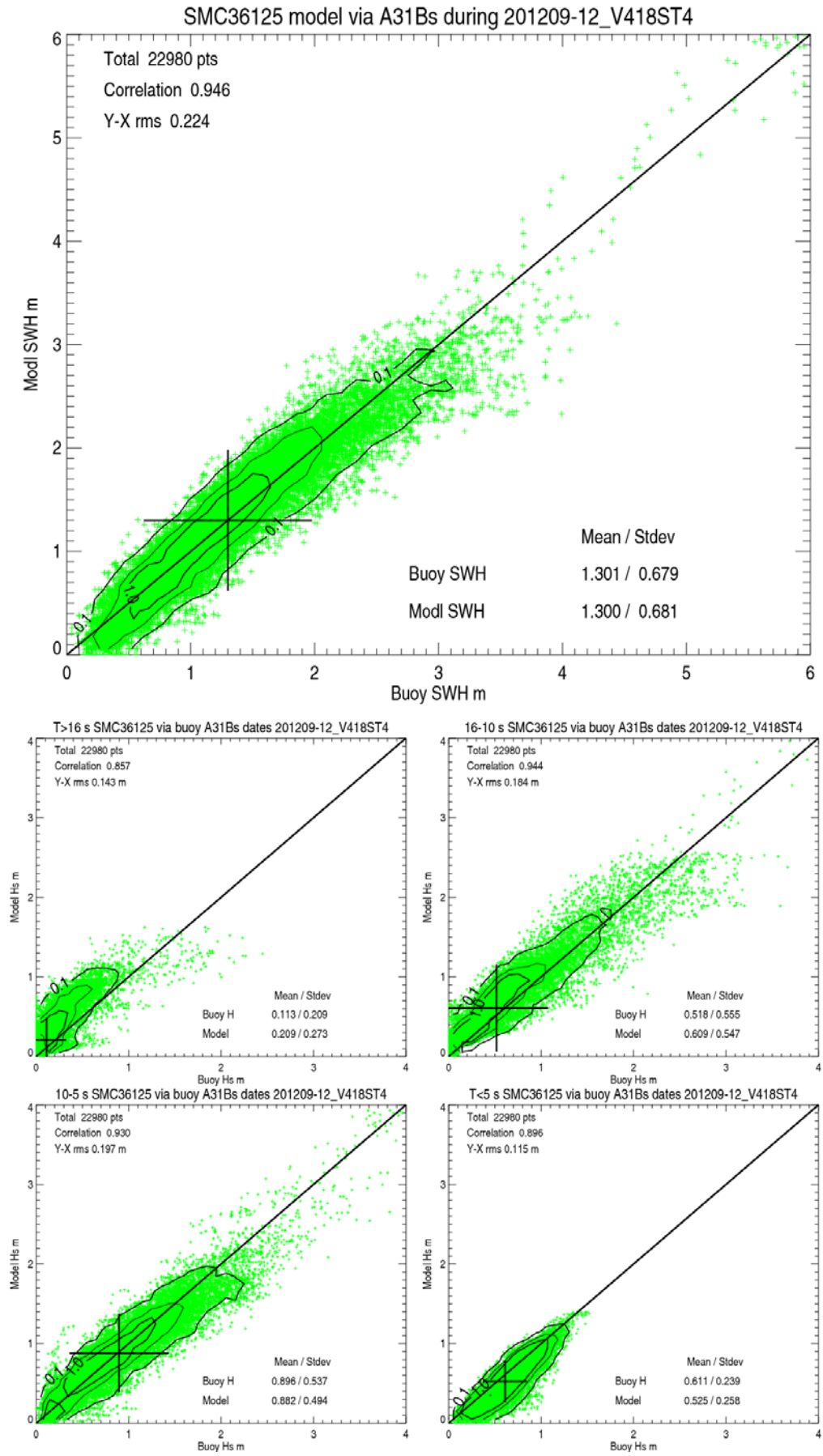


Fig.8. Comparison of SMC36125 model SWH and 4-bin sub-range wave height with buoy observations over 4 months from September to December 2012.

The relatively low correlation (0.74) between the model SWH and satellite measurement may be attributed to the following two factors: i) the SWH in comparison with the global average is relatively low within the polar region; ii) a proportionally more satellite data are likely to be contaminated by floating sea ice and coastal lands in the Arctic than in large ocean basins. Although the 4m-filter is applied it is not sufficient to remove all the erroneous altimeter data as shown in the scatter plots. Nevertheless, the influence is relatively small comparing with the majority of satellite data as indicated by the probability density function (pdf) contour lines in Fig.7. The pdf contour levels are set at 0.02, 0.1, 0.5 and 2.5% with 80 bins for the 0-8 m range in each dimension. Furthermore, the satellite observation is used as an intermediary ‘ruler’ to measure the differences between the two models so small errors in the data set are not very important as long as they are the same for both models. The linear correlation between the satellite data and model SWH would be improved if the comparison was extended to the whole globe due to inclusion of some high waves, especially from the Southern Oceans. However, it would shelter off the subtle differences between the two models.

The three models (SMC36125, SMC25Arc and SMC25Axp) are also validated against some spectral buoy observations. The spectral buoy positions are shown in Li (2012 Fig.4) and they all are located outside the polar region. As a result, both the Arc and Axp models yield identical scatter plots with the buoy data. The SMC36125 model shows a slightly better agreement with the buoy spectra than the SMC25 models because of the refined coastlines. The difference is similar to that of the SMC25 and SMC6-25 models as listed in Li (2012 Table 1) though the SMC36125 model results are even better than those of SMC6-25. Please note that the Arctic part is not activated for both SMC25 and SMC6-25 models in Li (2012). Here the SMC36125 model has an active Arctic part and one more refined level (3km) around the European coastlines than the SMC6-25 model. Besides, this study uses the latest public release of WAVEWATCH III Version 4.18 (Tolman and WDG, 2014) with some source term updates. Fig.8 shows the buoy 4-bin sub-range wave height (SRWH) scatter plots (bottom 4 panels) against the SMC36125 model over 4 months (August-December 2012). The SRWH is defined in analogue to the SWH but integrated over a limited frequency range (Li and Saulter, 2014). The 4-bin margins are marked with wave period  $T > 16$  s, 16-10 s, 10-5 s and  $T < 5$  s, respectively. The agreement is satisfactory over the whole wave spectral range though model swell is slightly higher than the buoy measurement (first bin  $T > 16$  s). The model wind sea is, however, slightly lower than the buoy value (forth bin  $T < 5$  s) and this partially cancels the model extra swell in the total wave energy budget. In fact, the total wave energy or SWH scatter plot (top panel in Fig.8) yields a better agreement than the 4-bin individual plots. The model mean SWH (1.30 m) matches exactly with the buoy one. This example illustrates the usefulness of the spectral breakdown of wave energy into SRWH in comparison with the total wave energy or SWH. Actually, the local tuning of the source term is carried out with the aid of the 4-bin SRWH. The wind sea input rate is tuned by comparing the  $T < 5$  s bin with buoy observations and the swell dissipation is checked with the  $T > 16$  s bin. Although this buoy comparison could not be used as a direct validation of the Arctic part, it reveals that the Arctic part is not affecting the global part if compared with the same buoy plot Fig.4 of Li and Saulter (2014), where the Arctic part was not activated.

## 5. Summary and conclusions

A SMC grid (Li, 2011, 2012) has been installed in the WAVEWATCH III® model and is included in the last public released version 4.18 (Tolman and WDG, 2014). The SMC grid relaxes the CFL restriction at high latitudes by merging the longitudinal cells and removes the polar singularity by introducing a round polar cell. The unstructured nature of the SMC grid allows all land cells to be removed out of wave propagation and refined resolutions near coastlines or in any region of interest. The time step relaxation at high latitudes and the use of sub-time steps for refined resolutions result in

a substantial computing cost reduction in comparison with a conventional latitude-longitude grid model.

A simple solution to the polar problem, caused by the rapid change of local east directions over merged cells or on a reduced grid, has also been applied. A map-east reference direction is introduced to define vector wave spectral components in a small polar region (Arctic part), so that the scalar assumption can be maintained at high latitudes. This method makes it possible to expand global wave models to cover the whole Arctic in response to the Arctic sea ice retreat in future summers. The map-east method is demonstrated with ocean surface wave modelling in an ice-free Arctic and is directly validated with available satellite observations in an expanded configuration.

Results of model-model comparisons and validation against satellite data indicate that the map-east method works in the polar region and is consistent with the conventional local east method between 65°N and 85°N. Transition between parts of the grid using the two different direction systems is seamless and smooth. Correlation of model and satellite SWH in the Arctic region was found to be generally lower than that for the full global comparison, but this is primarily due to the quality of satellite observations, rather than the wave model grid scheme. Comparison of model and buoy wave spectra using the 4-bin sub-range wave height SRWH shows that the global model is consistent when the Arctic part is included. This study also confirms that the multi-resolution SMC36125 grid is better than the single resolution ones in the full range of the ocean surface waves.

**Acknowledgements:** The author is grateful to Dr Andrew Saulter, Met Office, and others for their constructive suggestions to improve this article.

## References

- Ardhuin, F., E. Rogers, A. Babanin, J.F. Filipot, R. Magne, A. Roland, A. van der Westhuysen, P. Queffeulou, J.M. Lefevre, L. Aouf, F. Collard, 2010. Semiempirical dissipation source functions for ocean waves: Part I, Definition, calibration and validation. *J. Phys. Oceanogr.* **40**, 1917-1941.
- N. Booij, N., L.H. Holthuijsen, 1987. Propagation of ocean waves in discrete spectral wave models. *J. Comput. Phys.* **68**, 307-326.
- Li, J.G., 2008. Upstream non-oscillatory advection schemes. *Mon. Wea. Rev.* **136**, 4709-4729.
- Li, J.G., 2011. Global transport on a spherical multiple-cell grid. *Mon. Wea. Rev.* **139**, 1536-1555.
- Li, J.G., 2012. Propagation of ocean surface waves on a spherical multiple-cell grid. *J. Comput. Phys.* **231**, 8262-8277.
- Li, J.G., M. Holt, 2009. Comparison of ENVISAT ASAR ocean wave spectra with buoys and altimeter data via a wave model. *J. Atmos. Oceanic Techno.* **26**, 593-614.
- Li, J.G., A. Saulter, 2012. Assessment of the updated Envisat ASAR ocean surface wave spectra with buoy and altimeter data. *Remote Sensing of Environment* **126**, 72-83.
- Li, J.G., A. Saulter, 2014. Unified Global and Regional Wave Model on a Multi-Resolution Grid. *Ocean Dynamics* **64**, 1657-1670.
- Popinet, S., R. M. Gorman, G. J. Rickard, H. L. Tolman, 2010. A quadtree-adaptive spectral wave model. *Ocean Modelling* **34**, 36-49.
- Rasch, P.J., 1994. Conservative shape-preserving two-dimensional transport on a spherical reduced grid. *Mon. Wea. Rev.* **122**, 1337-1350.
- Roe, P.L., 1985. Large scale computations in fluid mechanics. in: E. Engquist, S. Osher, R.J.C. Somerville (Eds.), *Lectures in Applied Mathematics* **22**, 163-193.
- Tolman, H.L., 1991. A third-generation model for wind waves on slowly varying unsteady and inhomogeneous depths and currents. *J. Phys. Oceanogr.* **21**, 782-792.

- Tolman, H.L., 2003. Treatment of unresolved islands and ice in wind wave models. *Ocean Modelling*, **5**, 219-231.
- Tolman, H.L., 2008. A mosaic approach to wind wave modeling. *Ocean Modelling*, **25**, 35-47.
- Tolman, H.L., B. Balasubramanian, L.D. Burroughs, D.V. Chalikov, Y.Y. Chao, H.S. Chen, V.M. Gerald, 2002. Development and implementation of wind-generated ocean surface wave models at NCEP. *Weather and Forecasting*, **17**, 311-333.
- Tolman, H.L. and the WAVEWATCH III® Development Group, 2014. User manual and system documentation of WAVEWATCH III® V4.18. *Technical Note* **316**, NOAA/NCEP, 311 pp.
- Wang, M., J.E. Overland, 2009. A sea ice free summer Arctic within 30 years? *Geophys. Res. Lett.* **36**, L07502, 5pp.